Crossed-Wire Laser Microwelding of Pt-10 Pct Ir to 316 Low-Carbon Vacuum Melted Stainless Steel: Part I. Mechanism of Joint Formation

G.S. ZOU, Y.D. HUANG, A. PEQUEGNAT, X.G. LI, M.I. KHAN, and Y. ZHOU

The excellent biocompatibility and corrosion properties of Pt alloys and 316 low-carbon vacuum melted (LVM) stainless steel (SS) make them attractive for biomedical applications. With the increasing complexity of medical devices and in order to lower costs, the challenge of joining dissimilar materials arises. In this study, laser microwelding (LMW) of crossed Pt-10 pct Ir to 316 LVM SS wires was performed and the weldability of these materials was determined. The joint geometry, joining mechanism, joint breaking force (JBF), and fracture modes were investigated using optical microscopy, scanning electron microscopy (SEM), energy-dispersive X-ray spectroscopy (EDX), and microtensile testing. It was shown that the mechanisms of joint formation transitioned from (1) brazing, (2) a combination of brazing and fusion welding, and (3) fusion welding with increasing pulsed laser energy. The joints demonstrated various tensile failure modes including (1) interfacial failure below a peak power of 0.24 kW, (2) partial interfacial failure that propagated into the Pt-Ir wire, (3) failure in the Pt-Ir wire, and (4) failure in the SS wire due to porosity and severe undercutting caused by overwelding. During this study, the optimal laser peak power range was identified to produce joints with good joint geometry and 90 pct of the tensile strength of the Pt-10 pct Ir wire.

DOI: 10.1007/s11661-011-0763-3

I. INTRODUCTION

IN the fabrication of medical and electrical devices, thin metal sheets or wires (*i.e.*, 0.2- to 0.5-mm thickness) are often required.[1,2] Resistance microwelding (RMW) and laser microwelding (LMW) are two of the most common joining processes used for such microscale fabrication.[2–5] Recent literature on microwelding of crossed wires or sheet to sheet, such as Ni sheets, bare and Au-plated Ni wires, 316 low-carbon vacuum melted (LVM) stainless steel (SS), and 304 SUS SS wires have focused on the RMW process.[2,6–9] For example, Khan *et al.*[9] detailed the RMW joint formation mechanism and fracture modes of crossed 316 LVM wires. However, the increased complexity of medical devices has brought forth renewed challenges in the welding of dissimilar biocompatible materials. One such challenge when joining dissimilar materials is the variation in resistivity of materials, which has hindered the RMW of dissimilar alloys.[10] This highlights the need for more research on dissimilar joining using LMW. LMW offers advantages such as precision, no contact with work pieces, small HAZ, and consistent and reliable joints. Therefore, LMW has been widely applied to manufacturing various medical products such as pacemakers, defibrillators, catheters, cochlear implants, insulin pumps, stents, and orthopedic implants.[11,12]

The excellent corrosion resistance, biocompatibility, conductivity, and mechanical properties of Pt alloys and 316 LVM SS make them attractive for biomedical applications. For example, 316 LVM SS is used for wires, stents, batteries, and capacitor cases, while Pt and Pt alloys are used for coils, electrodes, and pins in electronic medical devices.[11,12] In recent years, several researchers reported both the LMW of Pt-Ir to Ti-6Al-4V alloy, the 316 LVM wire to itself, and the RMW of pure Pt to 316 LVM SS sheet.[10,12,13] The laser weldability of Pt-Ir to Ti alloy was found to be poor due to the formation of brittle intermetallic compounds such as Ti_3Pt and TiPt resulting in cracking.[12] Strong and smooth joints were made with 316 LVM wires under optimal laser energy input.[10] Chen[13] detailed the RMW joint formation mechanism and fracture mode of pure Pt wire to 316 LVM thin sheets. However, the RMW joint surface of pure Pt wire to 316 LVM sheet was found to be poor owing to the welding force. To present, no report on LMW of Pt-Ir alloy to 316 LVM wires has been found. The objective of this study is to identify the crossed-wire laser weldability of Pt-10 pct Ir to 316 LVM SS. The present article is

G.S. ZOU, Professor, is with the Department of Mechanical Engineering, Tsinghua University, Beijing 100084, People's Republic of China, and is also a Visiting Professor with the Department of Mechanical and Mechatronics Engineering, University of Waterloo, Waterloo, ON N2L 3G1, Canada. Y.D. HUANG, Visiting Student, is with the Department of Mechanical and Mechatronics Engineering, University of Waterloo, and is also a PhD Student with the State Key Laboratory of Advanced Welding and Joining, Harbin Institute of Technology, Harbin 150001, People's Republic of China. A. PEQUEGNAT, PhD Student, X.G. LI, Researcher/Technician, M.I. KHAN, Postdoctor, and Y. ZHOU, Professor, are with the Department of Mechanical and Mechatronics Engineering, University of Waterloo. Contact e-mail: apequegn@uwaterloo.ca
Manuscript submitted September 2, 2010.
Article published online June 18, 2011

focused on detailing the effects of pulsed-laser peak power on the weld geometry, joining mechanism, joint strength, and fracture mode.

In the joining of dissimilar crossed wires, it is expected that the orientation or stacking order will have a significant effect on the joining behavior due to differences in material properties such as melting temperature. The Pt-10 pct Ir alloy and the 316 LVM SS materials have a difference in melting temperature of 280 °C, where the melting temperatures of Pt-10 pct Ir and 316 LVM SS are 2053 K and 1773 K (1780 °C and 1500 °C), respectively. This article examines the case where the low melting point material (*i.e.*, 316 LVM SS) is on top and subject to laser energy. A companion article presents the results when the higher melting point material (*i.e.*, Pt-10 pct Ir wire) is on top.

II. EXPERIMENTAL PROCEDURES

Pt-10 pct Ir (wt pct) wire and cold-worked 316 LVM SS wire, both of 0.38-mm diameter, were joined in this study. The chemical composition of the 316 LVM SS wire is listed in Table I. The wires were ultrasonically cleaned in acetone prior to welding. Welding was conducted using a Miyachi Unitek LW-50A laser welding system (Miyachi Unitek Corporation, Monrovia, CA) capable of 50 J pulse energy and 5 kW peak power. A simple rectangular pulse profile was used for all welds with a nominal 0-ms upslope, 30-ms weld time, and 0-ms down slope. The optics used in this study produced a beam with a focused spot size of 400 μm and a Gaussian spatial profile. Peak power during welding was varied from 0.18 to 0.41 kW with an increment of 0.01 to 0.02 kW. An argon shielding gas was used during welding.

Figure 1 shows a schematic of the fixture used to locate the wires at right angles (90 deg). A hole in the fixture was located directly below the weld location to prevent welding of the wires to the fixture. The hole size was optimized with a depth of H = 1 mm and a diameter of Φ = 1 mm in order to achieve acceptable joint geometries with acceptable setdown of the 316 LVM SS wire. The fixture uses spring plates to apply a small force on the wires to promote intimate contact between the wires and to achieve adequate setdown of the top wire. A positioning laser was used to accurately center the beam on the intercept of the wires. This article describes only the results of LMW of crossed wires with 316 SS on top as the direct receptor of laser energy. The behavior of the alternate arrangement in which the Pt-Ir alloy is on top and directly laser heated is described in a companion article.

Table I. Chemical Composition of 316 LVM SS Wire (Weight Percent)

C	Mn	Si	Cr	Ni	Mo	P	S	Cu	N	Fe
0.024	1.84	0.75	17.47	14.73	2.76	0.017	0.001	0.04	0.024	bal

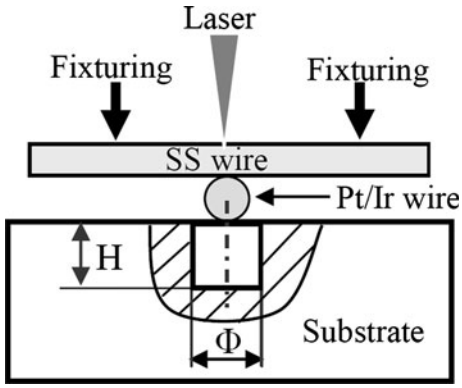

Fig. 1—Schematic of welding fixture, where H = 1 mm and Φ = 1 mm (not to scale).

Figure 2 shows the typical joint shape, in which φ_o and S represent the diameter of the 316 LVM wire close to the weld and the covered depth of Pt-Ir wire by 316 LVM SS, respectively. The S value was measured through SEM images of joint cross sections. The ratio of covered depth (R_c) was calculated by

$$R_c = S/\varphi_o \times 100 \text{ pct} \quad [1]$$

A schematic of the tensile testing method used to determine the joint breaking force (JBF) is shown in Figure 3. Tensile tests were performed using an INSTRON* model 5548 microtensile tester with a

*INSTRON is a trademark of Instron, Canton, MA.

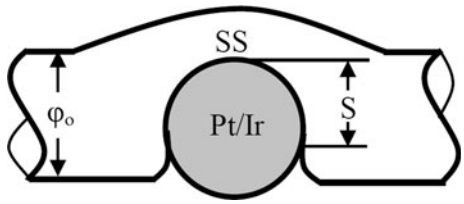

Fig. 2—Schematic of typical joint shape.

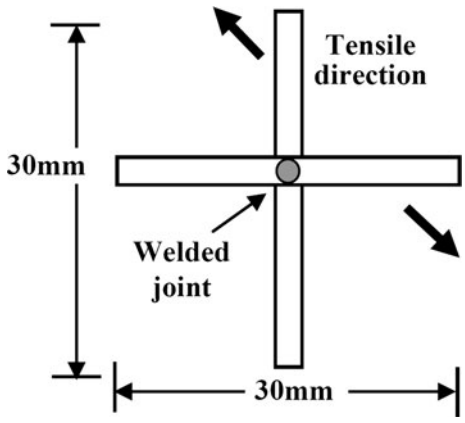

Fig. 3—Schematic of tensile test setup (not to scale). The large arrows indicate the direction of the applied tensile force. The joint is tested under a tensile-shear condition.

crosshead speed of 4 mm/min. Three joints were tested for each set of welding parameters to obtain the average JBF.

The geometry, fracture surfaces, and cross sections of joints were observed using optical microcopy and scanning electron microscopy (SEM). Vickers hardness tests were performed on joint cross sections with a load of 50 g and holding time of 15 seconds.

III. RESULTS

A. *Weld Geometry*

SEM images of the top and bottom of crossed-wire joints made at various different peak powers are shown in Figures 4(a) through (f). The SS wire that was subject to the incident laser beam (*i.e.*, the wire that was on top) melts first and wets the Pt-Ir wire. Little wetting of the Pt-Ir wire with molten SS was observed at low powers, as shown in Figures 4(a1) and (a2) for a peak power of 0.21 kW. However, with increasing peak power, wetting of the Pt-Ir wire became more extensive (Figures 4(b1) through (d1) and (b2) through (d2)). Complete wetting of the Pt-Ir wire is shown in Figures 4(d1) and (d2), where a peak power of 0.36 kW was used. The cross section made along the SS wire in Figure 5(a) shows that nearly full setdown of the SS wire was achieved with a peak power of 0.25 kW; however, due to poor wetting, a notch remained on either side of the Pt-Ir wire. A significant increase in wetting was observed in the sample joined with 0.29-kW peak power where a fillet was formed between the molten SS and the Pt-Ir wire, as shown in Figure 5(b). Overwelding occurred when using peak powers above 0.39 kW, as shown in Figures 4(e1) through (f1) and (e2) through (f2). Large pores were formed and undercutting became severe, which often resulted in the SS wire breaking under the load of the fixture during solidification.

B. *Joint Cross Sections and Microstructure Analysis*

High- and low-magnification SEM images of the joint interfaces are shown in Figures 6 through 11. Using peak powers below 0.24 kW, no visible reaction layer was observed at the joint interface, as shown in Figure 6, most likely due to the very short welding time (*i.e.*, 30 ms) and relatively low brazing temperature produced under low energy input. Increasing peak power to 0.27 kW, as shown in Figure 8, resulted in a coarse reaction layer and the onset of fusion welding at the interface at the top of the joint. A columnar dendritic structure was observed to grow perpendicular to the fusion boundary, as shown in Figures 8 through 10. Layers of unmixed Pt-Ir material were observed in the SS weld pool, as indicated by points P1 and P2 in Figure 10(a), where a peak power of 0.35 kW was used. This higher Pt and Ir content in the unmixed layers for the 0.35 kW sample was confirmed by energy-dispersive X-ray spectroscopy (EDX), as detailed in Table II. Increasing peak power led to higher content of Pt and Ir in the fusion zone (FZ), as shown by the microstructural

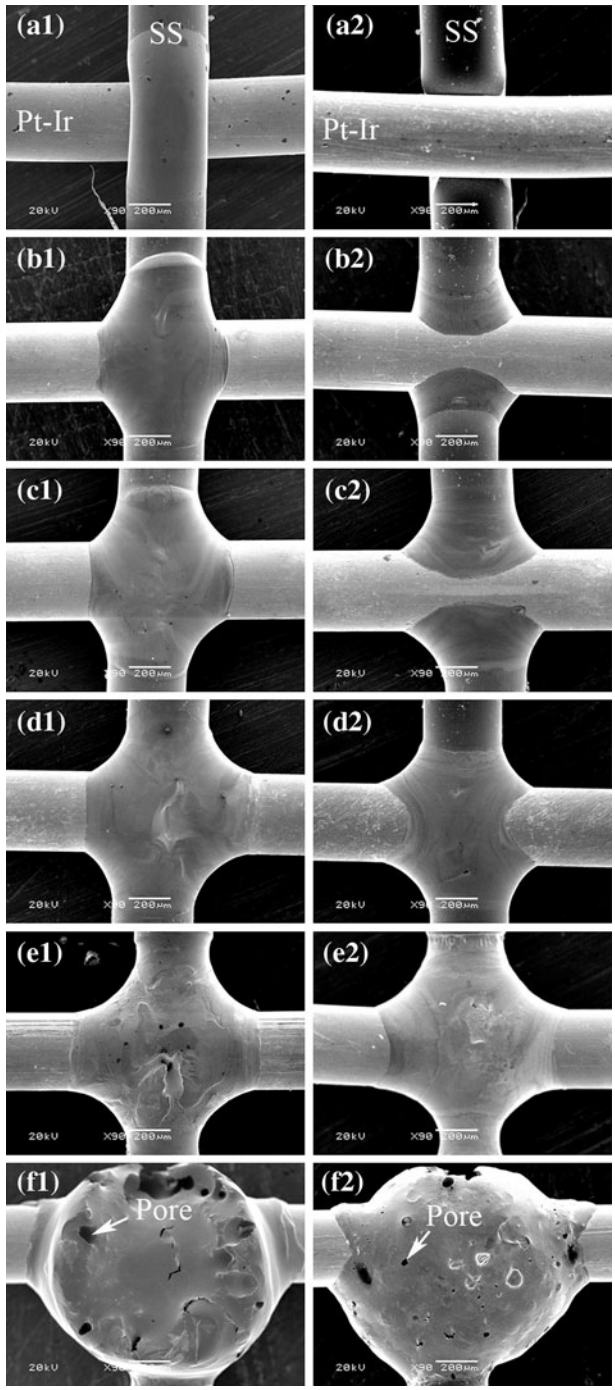

Fig. 4—Top (a1) to (f1) and bottom (a2) to (f2) surfaces of welded crossed-wire joints with laser peak powers of (*a*) 0.21 kW, (*b*) 0.29 kW, (*c*) 0.35 kW, (*d*) 0.36 kW, (*e*) 0.39 kW, and (*f*) 0.41 kW.

contrast in the backscattered SEM images and confirmed by EDX analysis in Table II. Increasing the peak power further to 0.39 to 0.40 kW resulted in complete melting of the Pt-Ir wire in the FZ, where complete mixing occurred. Once complete melting of the joint occurred, porosity began to occur, as shown in Figure 11(b). Overwelding was observed with peak powers above 0.41 kW, where the SS wire would break on occasion and pores of various sizes were produced, as shown in Figure 4(f).

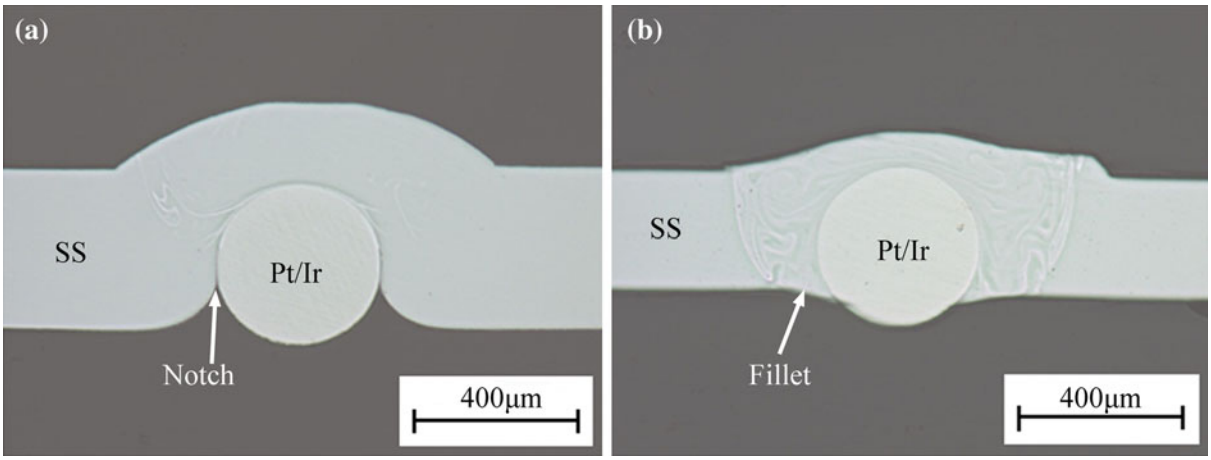

Fig. 5—Optical images of cross sections made along the 316 LVM SS wire for joints made with peak powers of (*a*) 0.25 kW and (*b*) 0.29 kW.

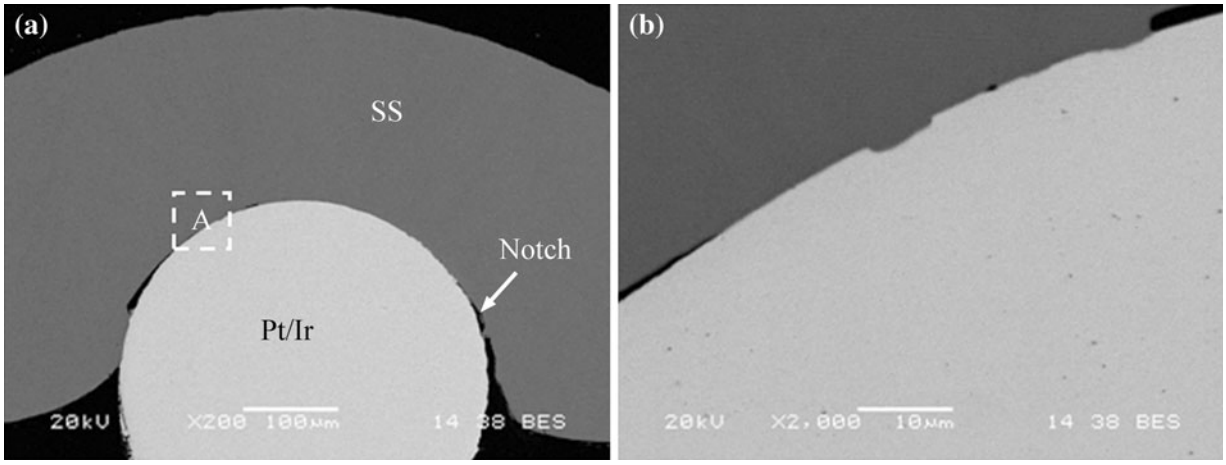

Fig. 6—(*a*) Cross-section images of joint produced with a peak power of 0.22 kW. (*b*) High-magnification image of region A.

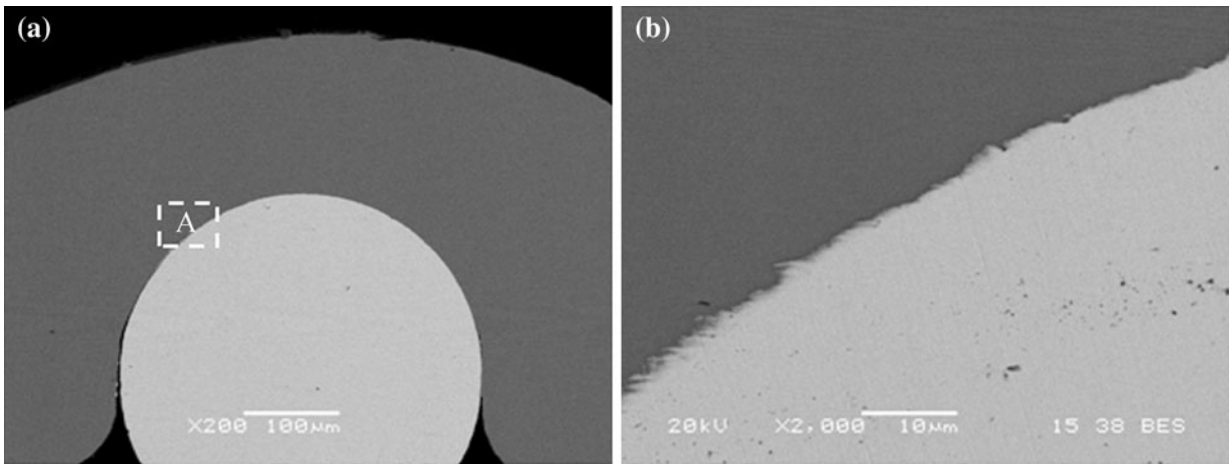

Fig. 7—(*a*) Cross-section images of joint produced with a peak power of 0.24 kW. (*b*) High-magnification image of region A.

C. *Microhardness*

Microhardness tests were performed on joints cross sectioned along the Pt-Ir wire and SS wire axis directions, as shown in Figures 12 and 13, respectively. Figure 12(a) shows a fusion-welded joint produced with peak power of 0.39 kW, and Figure 13(b) shows a mixed braze and fusion-welded joint produced with a peak power of 0.35 kW. The hardness of the base

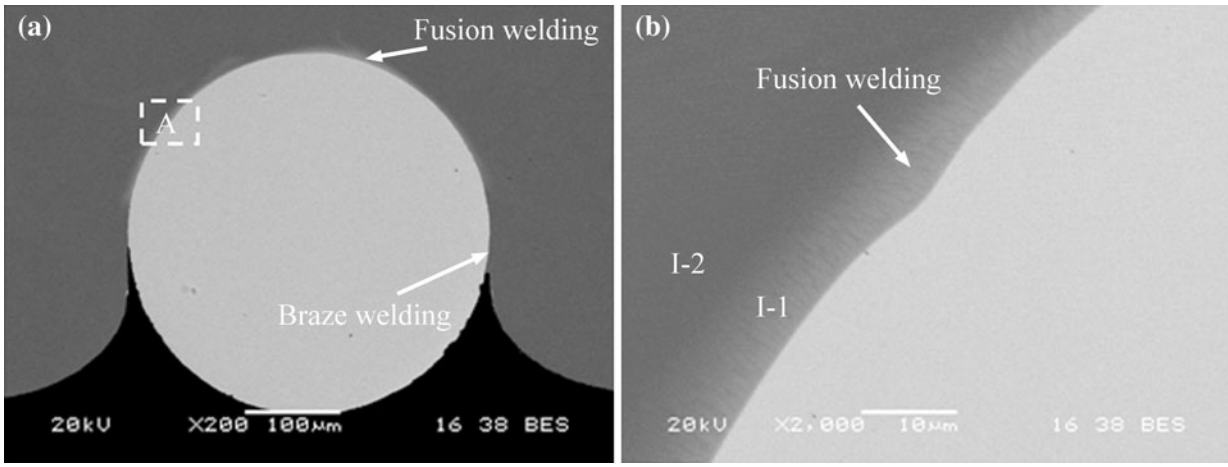

Fig. 8—(*a*) Cross-section images of joint produced with a peak power of 0.27 kW. (*b*) High-magnification image of region A.

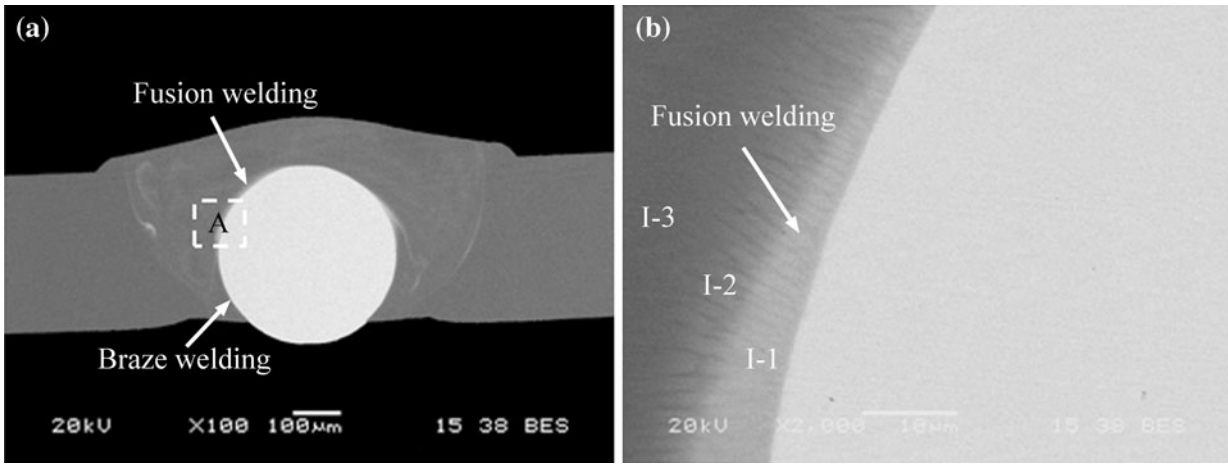

Fig. 9—(*a*) Cross-section images of joint produced with a peak power of 0.33 kW. (*b*) High-magnification image of region A.

Pt-10 pct Ir wire and 316 LVM SS wires were 140 to 160 HV and 380 to 420 HV, respectively.

Only slight softening in the heat-affected zone (HAZ) of the Pt-Ir was found in this study, as shown in Figures 12(a) and (b) just outside of the fusion boundary. In comparison, the softened region of the SS wire was larger and severe softening was identified. The hardness decreased from about 400 to 200 HV in the SS material, as shown in Figure 13(b). Similar softening in SS materials was reported in the literature.[7–9] Khan *et al.*[9] found that the microhardnesses of the HAZ and FZ were similar when welding 316 LVM SS using the RMW process. The original work-hardened structure of the SS wire was lost due to the thermal cycle of the welding process, leading to recrystallization and resolidification of the microstructure in the HAZ and FZ, respectively. Distinguishing between the resolidified SS material and the HAZ, therefore, was difficult, as was found in this study. Etching of the samples to identify changes in the microstructure was also not possible due to a galvanic couple between the noble Pt-10 pct Ir wire and SS wire. Excessive pitting of the SS material occurred, rendering microstructural analysis impossible.

D. *JBF and Fracture Mode*

The R_c and JBF as a function of peak power are summarized in Figures 14(a) and (b), respectively. A minimum peak power of 0.22 kW was required to form a joint strong enough for tensile testing. The dramatic increase in JBF of joints produced with increasing peak power from 0.22 and 0.26 kW was attributed to the increase in both bonded area and interfacial bond strength. The increase in bonded area was evident by observing the increase in the R_c value, as shown in Figure 14(a). The strength of the bond interface increased as the joint transitioned from a braze type joint, where molten SS wetted the unmolten Pt-Ir wire, to a fusion weld, where both wire materials were molten. A relatively stable JBF of approximately 38.5 N (*i.e.*, 90 pct of the 43 N tensile strength of the Pt-10 pct Ir wire) was obtained when the peak power was in the range of 0.26 to 0.39 kW. The average JBF reduced and the standard deviation became very large when using peak powers above 0.39 kW. At this point, overwelding occurred, resulting in porosity and severe undercutting in the SS wire. The SS wire was broken by overwelding,

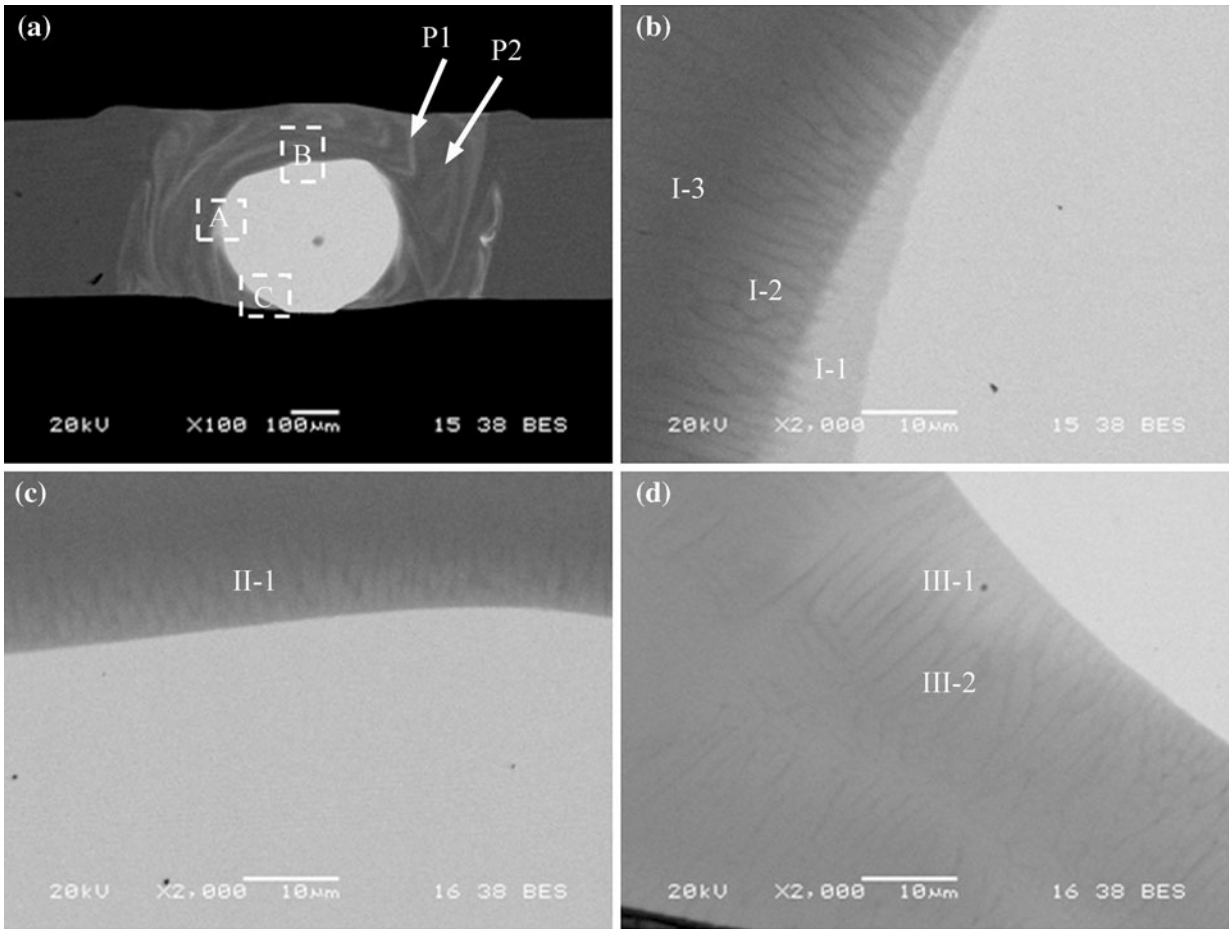

Fig. 10—(*a*) Cross-section images of joint produced with a peak power of 0.35 kW. High-magnification images of regions (*b*) A, (*c*) B, and (*d*) C.

Table II. EDX Analysis Results of Joint Cross Sections (Atomic Percent)

Joints	Position	Si	Cr	Mn	Fe	Ni	Mo	Ir	Pt
0.27 kW	I-1	—	15.8	1.2	55.5	13.1	0.9	1.5	12.0
	I-2	2.0	17.1	1.9	62.1	13.9	2.1	0.3	0.2
0.33 kW	I-1	—	15.9	2.4	44.3	7.3	1.5	2.7	25.9
	I-2	0.9	16.0	2.6	58.6	12.9	1.9	1.3	5.8
	I-3	1.2	17.6	1.9	59.4	15.6	2.6	0.2	1.5
0.35 kW	I-1	—	10.2	0.5	26.8	8.3	1.3	7.3	45.6
	I-2	—	17.5	1.7	53.3	13.1	2.4	1.6	10.4
	I-3	0.9	20.4	0.8	56.8	14.7	1.5	0.3	4.5
	II-1	1.8	16.8	1.2	50.3	12.3	0.5	0.9	16.2
	III-1	—	11.9	1.6	43.5	7.6	5.6	2.5	27.3
	III-2	—	17.7	1.2	54.5	9.8	2.1	2.7	12.0
	P1	1.3	14.7	1.4	59.6	12.6	1.4	1.0	8.0
	P2	1.1	19.0	2.5	60.3	13.8	1.9	0.6	0.8

and hence, the JBF was zero when the peak power surpassed 0.41 kW.

Figures 15(a) through (f) show the fracture surfaces of the joints produced at various peak powers. An interfacial failure occurred in joints produced with peak powers below 0.24 kW, as shown in Figures 15(a) and (b). This coincides well with the low R_c and JBF of joints produced using these low peak powers. The percentage of Pt-Ir remaining on the fractured sample was observed to increase with peak power. Joints made with peak powers between 0.24 and 0.27 kW had fracture initiate at the bonded interface and then propagate to the Pt-Ir wire, as shown in Figures 15(c) and (d). This was likely due to the increase in bonded area as higher peak power was applied. With further increase in peak power (0.28 to 0.39 kW), failure occurred completely in the Pt-Ir wire, as shown in Figure 15(e). At these power levels, the Pt-Ir wire was completely wetted by molten SS and

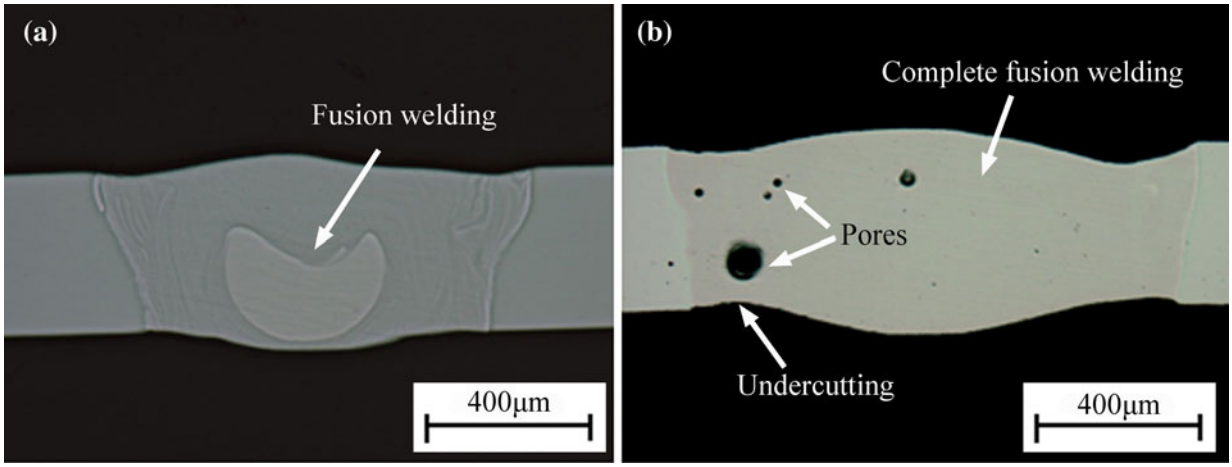

Fig. 11—Optical micrographs of cross-sectioned joints produced with peak powers of (*a*) 0.38 kW and (*b*) 0.40 kW.

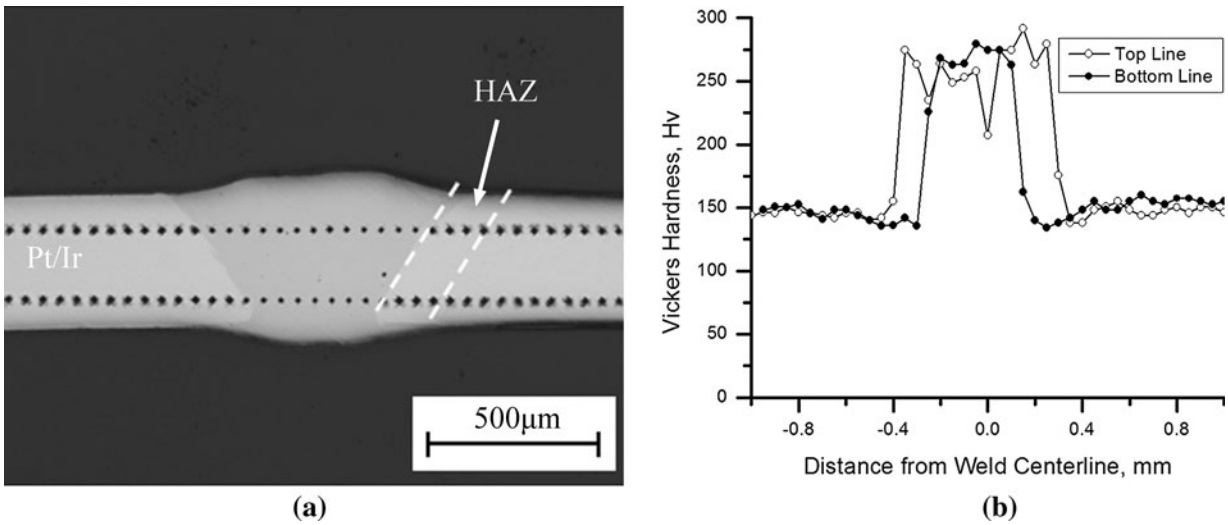

Fig. 12—Microhardness tests performed on 0.39 kW joint cross sectioned along the Pt-Ir wire axis direction: (*a*) optical image of sample and (*b*) Vickers hardness results.

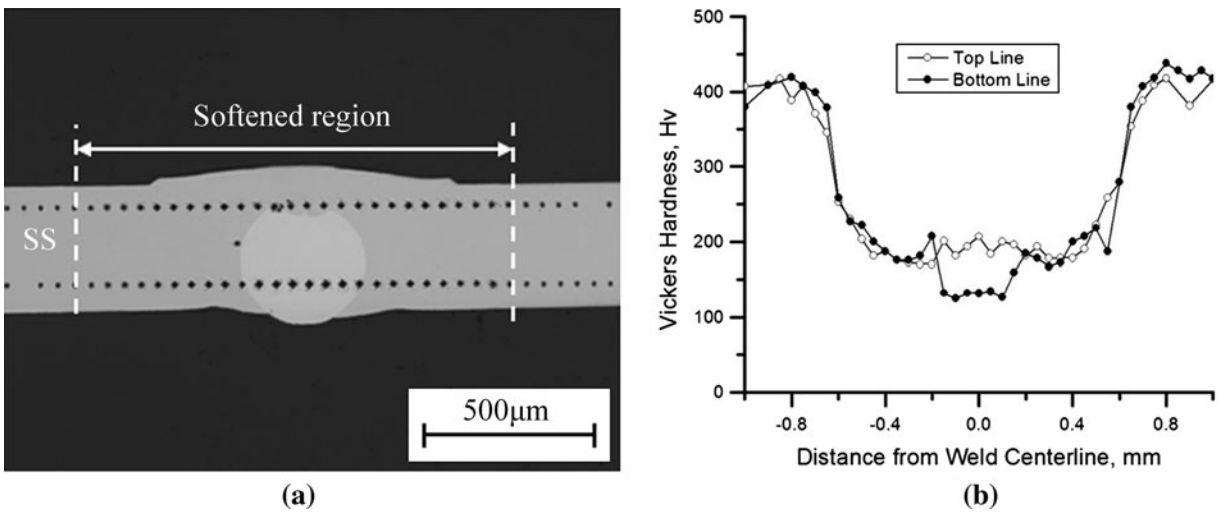

Fig. 13—Microhardness tests performed on 0.35 kW joint cross sectioned along the SS wire axis direction: (*a*) optical image of sample and (*b*) Vickers hardness results.

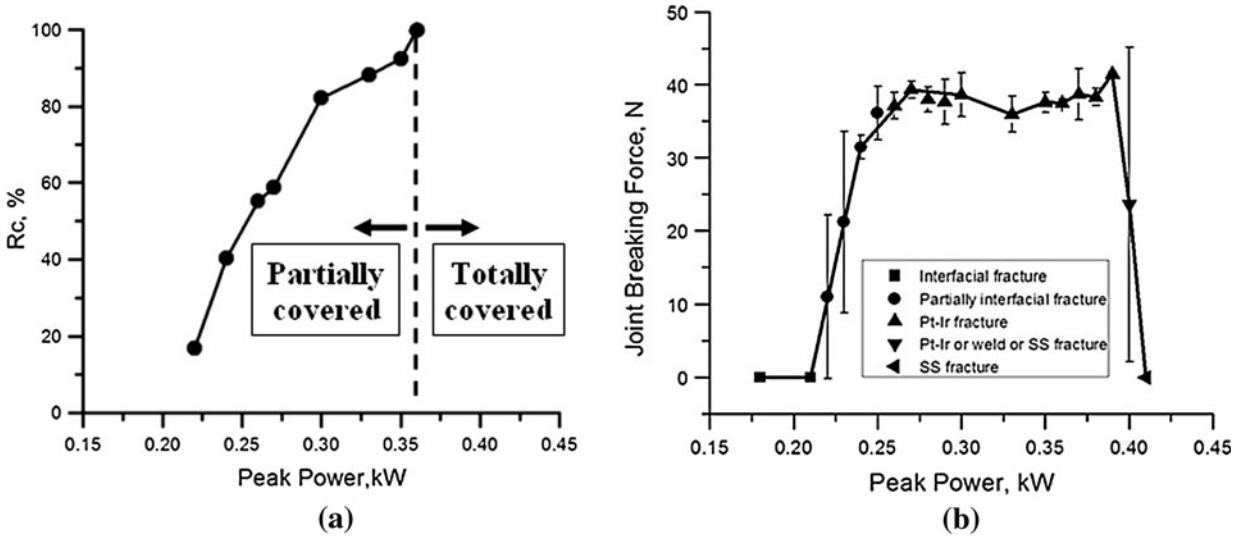

Fig. 14—Effects of peak power on (*a*) R_c and (*b*) JBF.

the notch at the bottom of the joint was gone. Once overwelding occurred above peak powers of 0.39 kW, failure occurred in the SS wire, where a combination of HAZ softening, severe undercutting, and porosity caused a reduction in strength.

IV. DISCUSSION

A. *Joining Mechanism*

In previous research concerning the RMW of small-scale sheets or wires, mechanisms of joint formation were discussed in detail.[2,6–9,13] Khan *et al.* showed that the joint formation mechanism of crossed 316 LVM wires during RMW was a combination of primary fusion welding and partial solid-state bonding when using relatively low welding force of 1.5 kg,[9] while the results of Fukumoto *et al.* demonstrated a mechanism of predominantly solid-state bonding at a higher welding force of 5.6 kg when welding SUS 304 SS wires.[8] Chen reported a progression of mechanisms including solid-state bonding, short-time brazing, and finally fusion welding when RMW was used to join pure Pt wire to 316 LVM sheet.[13] In contrast to the RMW process, Khan and Zhou emphasized that fusion welding was the key mechanism of joint formation in the LMW of 316 LVM crossed wires.[10] However, there is a lack of literature on the joining mechanism during the LMW of dissimilar materials in a crossed-wire configuration, as was performed in this study. The difference in material properties such as melting temperatures affects the joining mechanism, as discussed in the following paragraphs.

A schematic diagram of the joint formation is shown in Figure 16 to aid in the discussion. At low peak power levels (*i.e.*, <0.24 kW), formation of the joint began when the SS wire melted on top of the Pt-Ir wire in a reflow type laser-brazed joint. The molten SS was able to wet the surface of the Pt-Ir wire and form a short-time brazed joint, as indicated by "A" in Figure 16(a). The significant difference in melting temperatures of the 316 LVM SS wire and the Pt-10 pct Ir wire with melting points of 1773 K and 2053 K (1500 °C and 1780 °C), respectively, led to initial melting of only the SS wire that was subject to the incident laser beam. When only braze welding occurred, molten SS with insufficiently high temperature resulted in poor fluidity on the Pt-Ir surface and a low R_c value with notches on the bottom of the joint, as illustrated in Figure 16(a). It was noted that no interfacial bonding was able to occur if the SS wire was not melted through its diameter in LMW, in contrast to what was found in previous research with RMW. During RMW, local solid-state bonding at faying surfaces could be attained at relatively low welding current under the high welding force even though no melting was observed.[13] Solid-state bonding becomes possible due to the high clamping forces of the electrodes used in the RMW process.[13]

As the peak power is increased to between 0.25 and 0.28 kW, fusion welding started to occur at the top portion of the interface, as illustrated by "B" in Figure 16. At this location, the temperature reached the melting temperature of the Pt-Ir wire. The setdown or R_c value also increased as the wetting of the Pt-Ir wire with molten SS improved with the increase in the energy input. Further increasing the peak power to 0.29 to 0.38 kW produced a smooth joint with increased bonded area and bond strength. The notch illustrated in Figures 16(a) and (b) was replaced with an SS fillet as the peak power increased due to improved wetting, as illustrated in Figure 16(c). At this point, the failure mode of the joints transitioned to failure only in the Pt-Ir wire adjacent to the weld, as shown in Figure 15(e), due to better joint geometry and a larger bonded area.

Only fusion welding occurred with peak powers between 0.39 and 0.40 kW, as illustrated in Figure 16(e). Complete melting of the Pt-Ir wire occurred, and both external and internal pores were seen in the FZ. Further increasing the peak power above 0.41 kW led to overwelding, where large amounts of pores were formed

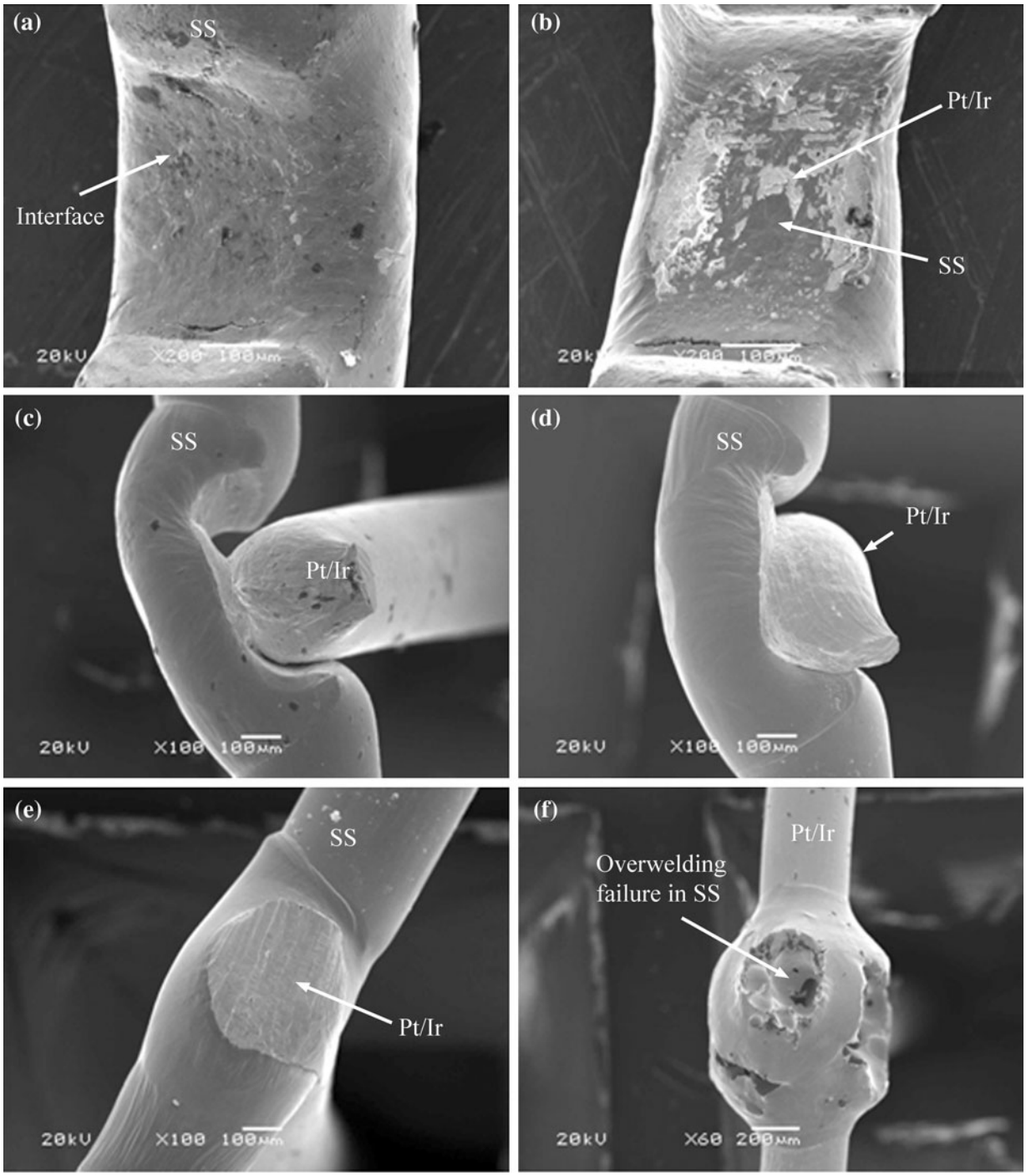

Fig. 15—SEM images of fracture surfaces in joints produced with peak powers of (*a*) 0.18 kW, (*b*) 0.22 kW, (*c*) 0.24 kW, (*d*) 0.27 kW, (*e*) 0.35 kW, and (*f*) 0.40 kW.

and severe undercutting occurred in the SS wire leading to breaking of the SS wire during solidification under the load of the fixture. The overwelded joint is illustrated in Figure 16(f).

B. *Optimum Welding Power*

Joints that failed mostly in the Pt-Ir wire adjacent to the weld had a JFB of 90 pct of the tensile strength of the base Pt-Ir wire. These joints were produced with peak powers within a relatively large range of 0.26 to 0.39 kW, as shown in Figure 14(b). However, in medical applications, such as stents made using 316 LVM SS wires, device electrodes, and pins using pure Pt or a Pt alloy, smooth joint surfaces are also critical in avoiding damage to tissues, as well as in producing uniform current transport through welds.[1,9,11,12] Therefore, for welding process optimization, both strength and

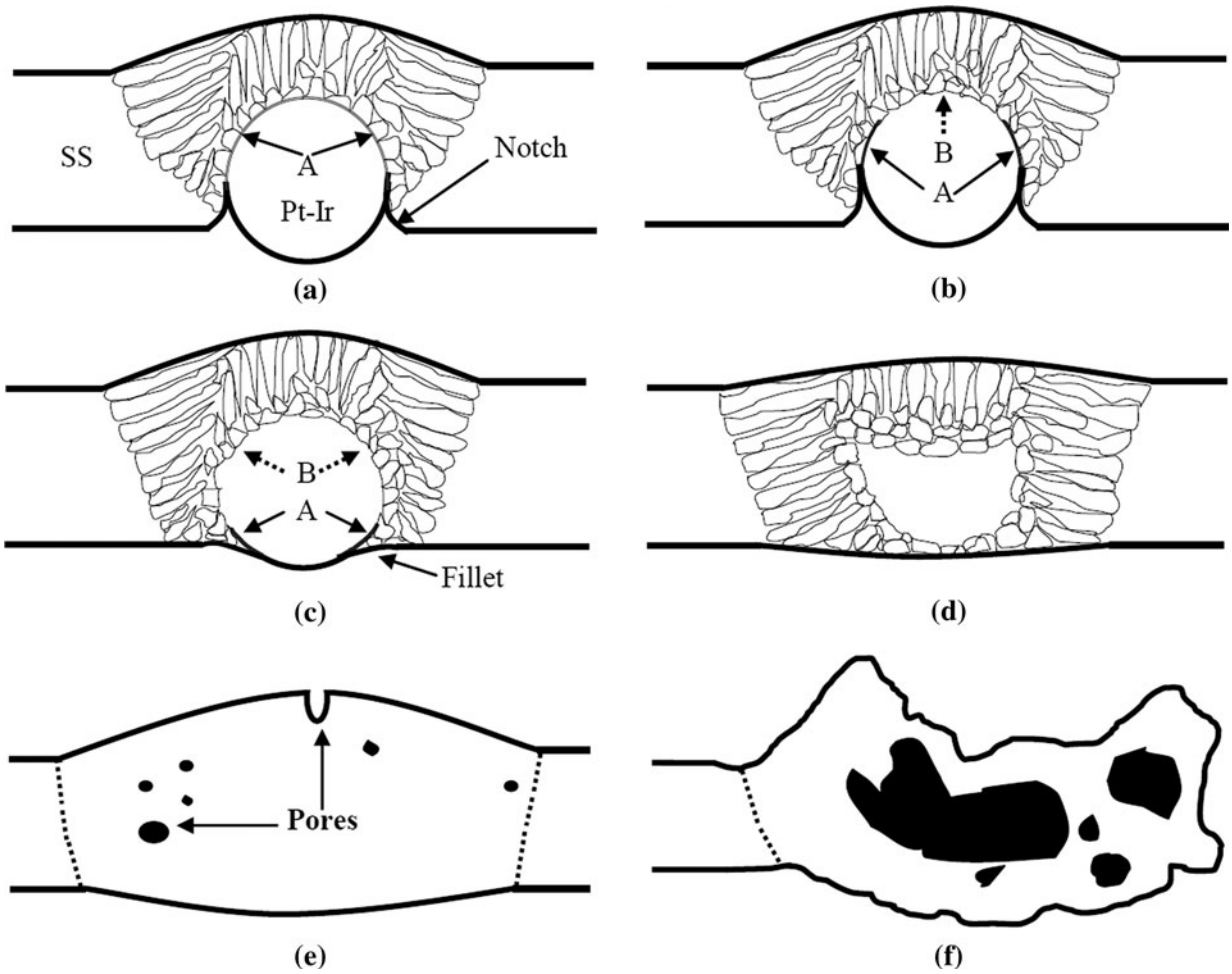

Fig. 16—Schematic of joining mechanism with increasing laser peak power. (*a*) Brazing (<0.24 kW), (*b*) and (*c*) combination of brazing and fusion welding (0.25 to 0.35 kW), (*d*) combination of brazing and fusion welding with complete wetting of Pt-Ir wire (0.36 to 0.38 kW), (*e*) fusion welding (0.39 to 0.40 kW), and (*f*) overwelding (>0.41 kW).

surfaces of joints should be evaluated. In the current study, peak powers of 0.29 to 0.38 kW were observed to produce ideal joints with the highest possible JBF along with smooth joint configuration due to good wetting of the Pt-Ir wire while having no internal or external porosity.

V. CONCLUSIONS

LMW of crossed Pt-10 pct Ir wire to 316 LVM SS wire was investigated by observing joint geometry, joining mechanism, JBF, and fracture modes. The main conclusions of this study are as follows.

1. With increasing peak power, the joining mechanism transitions from (a) brazing to (b) a combination of brazing and fusion welding and, finally, to (c) complete fusion welding. Brazing was found to occur with peak powers below 0.24 kW, while complete fusion welding was seen above a peak power of 0.38 kW.
2. Little HAZ softening occurred in the Pt-10 pct Ir wire, while a significant 200 HV decrease in hardness was measured in the HAZ and resolidified region of the 316 LVM SS wire.
3. Four different failure modes were identified with joints produced with increasing peak power during tensile testing. These include (a) interfacial failure below a peak power of 0.24 kW, (b) partial interfacial failure that propagated into the Pt-Ir wire, (c) failure in the Pt-Ir wire, and (d) failure in the SS wire due to porosity and severe undercutting caused by overwelding.
4. Approximately 90 pct of the 43 N tensile strength of the Pt-10 pct Ir wire can be achieved with welds produced within the optimum peak power range of 0.29 to 0.38 kW. These optimum parameters produce joints that fail in the Pt-Ir wire, giving them the highest JBF. These joints were found to have a smooth surface geometry with no porosity or notches.

ACKNOWLEDGMENTS

This work was funded by the Program of Canada Research Chairs (CRC) in Microjoining (www.crc.gc.ca).

A special thanks goes out to B. Tam for helping with the preparation of the welded samples. The help of Professor W.H.S. Lawson in reviewing this manuscript is greatly appreciated.

REFERENCES

1. Y. Zhou, ed.: *Microjoining and Nanojoining*, Woodhead Publishing Ltd., Cambridge, United Kingdom, 2008.
2. W. Tan, Y. Zhou, and H.W. Kerr: *Metall. Mater. Trans. A*, 2002, vol. 33A, pp. 2667–76.
3. K.J. Ely and Y. Zhou: *Sci. Technol. Weld. Join.*, 2001, vol. 6 (2), pp. 63–72.
4. R. Singh and N.B. Dahotre: *J. Mater. Sci.*, 2005, vol. 40 (21), pp. 5619–26.
5. D.R. Haynes, T.N. Crotti, and M.R. Haywood: *J. Biomed. Mater.*, 2000, vol. 49 (2), pp. 167–75.
6. S. Fukumoto and Y. Zhou: *Metall. Mater. Trans. A*, 2004, vol. 35A, pp. 3165–76.
7. S. Fukumoto, Z. Chen, and Y. Zhou: *Metall. Mater. Trans. A*, 2005, vol. 36A, pp. 2717–24.
8. S. Fukumoto, T. Matsuo, H. Tsubakino, and A. Yamamoto: *Mater. Trans.*, 2007, vol. 48 (4), pp. 813–20.
9. M.I. Khan, J.M. Kim, M.L. Kuntz, and Y. Zhou: *Metall. Mater. Trans. A*, 2009, vol. 40A, pp. 910–19.
10. I. Khan and Y. Zhou: *Proc. Materials and Processes for Medical Devices Conf. (MPMD)*, Palm Springs, CA, Sept. 2007.
11. J. Xie and S. Safarevich: *Proc. Materials and Process for Medical Devices Conf. (MPMD)*, Anehei, CA, Sept. 2003.
12. N.J. Noolu, H.W. Kerr, Y. Zhou, and J. Xie: *Mater. Sci. Eng. A*, 2005, vol. 397, pp. 8–15.
13. Z. Chen: *J. Mater. Sci.*, 2007, vol. 42, pp. 5756–65.